Available online at www.sciencedirect.com
ScienceDirect
Journal of Sound and Vibration 302 (2007) 88–103
JOURNAL OF SOUND AND VIBRATION
www.elsevier.com/locate/jsvi

Rotor/active magnetic bearing transient control using wavelet predictive moderation

Iain S. Cade*, Patrick S. Keogh, M. Necip Sahinkaya

Department of Mechanical Engineering, University of Bath, Bath, BA2 7AY, UK

Received 28 April 2006; received in revised form 14 November 2006; accepted 14 November 2006
Available online 26 January 2007

Abstract

A novel method for predicting the ultimate steady-state vibration amplitudes from measured transient responses in multi-input, multi-output flexible rotor/magnetic bearing systems is presented. The technique is based around a multi-level wavelet coefficient analysis with in-built transient system dynamics. The relation between an input disturbance wavelet coefficient acting on the system and a measured vibration wavelet coefficient is identified theoretically for non-identical wavelets. A controller is formulated in the wavelet coefficient domain with control forces derived from proportional feedback of displacement wavelet coefficients. Improved transient performance is achieved using wavelet coefficient steady-state prediction to moderate the control signal. Experimental validation of the controller using mass-loss tests demonstrates the manner in which transient vibration attenuation may be achieved.

1. Introduction

Magnetic bearings offer the ability to vary radial rotor force dynamically and are commonly used with a control strategy to attenuate vibrations levels during operation of rotating machinery. The origin of disturbance forces may be attributed to normal operating conditions or from a fault. Specific examples of disturbances include rotor unbalance, base acceleration and aerodynamic excitation.

There exist many methods of evaluating control forces from open- and closed loop strategies. Burrows and Sahinkaya [1] use open-loop techniques to identify the optimum control forces to minimise steady-state synchronous vibration. Simulations of sudden variation of rotor unbalance are considered by Shafai et al. [2] using an adaptive open-loop controller. Knospe et al. [3] present a method of adaptive open-loop updating of influence coefficients to identify control forces over several cycles. However, open-loop controllers designed to minimise steady-state vibration may be ineffective during transient vibration periods. Optimally designed controllers may improve system performance provided they are formulated from an accurate model of the system. An H_∞ derived controller was developed by Fujita et al. [4] for an experimental flexible rotor levitated by active magnetic bearings. Cole et al. [5] designed a controller that is robust to both direct rotor forcing and

*Corresponding author. Tel.: +44 1225 383057; fax: +44 1225 386928.
E-mail addresses: I.S.Cade@bath.ac.uk (I.S. Cade), P.S.Keogh@bath.ac.uk (P.S. Keogh), M.N.Sahinkaya@bath.ac.uk (M.N. Sahinkaya).

0022-460X/$ - see front matter © 2006 Elsevier Ltd. All rights reserved.
doi:10.1016/j.jsv.2006.11.005

base motion. Control of transient rotor vibration has been considered using H_∞ optimisation by Keogh et al. [6]. Further, μ-synthesis has been used to increase the accuracy involved in modelling the plant perturbations and errors in order to improve closed-loop performance [7]. Optimal model based controllers are, however, limited by the compromise between high system order and computational efficiency for real-time operation. In principle, if a controller could provide a perfect control signal at the same time as a change in the input disturbance then the rotor vibration would be zero. However, high system order limits the speed of response of the controllers. Synchronous and multi-frequency controllers offer a faster response time, but may provide inappropriate control forces during transient excitation.

In recent years wavelet analysis has been used to identify features and characteristics within a signal. Newland [8,9] presents a method of representing a recorded vibratory signal as a time–frequency map using wavelet analysis, while Staszewski [10] identifies damping characteristics from multi-degree-of-freedom models. The ridges and skeletons method proposed by Staszewski [11] is used to identify nonlinear systems. Chancey and Flowers [12] extract transient patterns from measured rotor vibrations. Zou et al. [13] determine features from a simulated cracked rotor passing through a subcritical speed from the transient response. Cade et al. [14] identify the onset time for a fault condition in a rotor/magnetic bearing system. Wavelet analysis has also been used to study fault conditions in rolling element bearings [15] and gearboxes [16]. Although it has been used extensively for identification, wavelet analysis has had relatively little use in real-time closed loop control applications. Parvez and Goa [17] use simple proportional wavelet coefficient feedback for specific bandwidths. However, system delays associated with control signal evaluation can cause instability. More recently, Cole et al. [18] developed a controller designed to attenuate transient and steady-state vibration using model-based integral wavelet coefficient feedback in a single measurement plane only.

Wavelet analysis has been demonstrated as a useful tool for understanding the dynamic response of a variety of systems. In particular, its ability to identify transient behaviour is of significant interest. This paper focuses on the use of wavelet analysis to identify steady-state characteristics from transient data in order to influence a control strategy acting in the wavelet coefficient domain. Multiple rotor measurement planes are also considered, which will generally result in residual vibration that may not be fully attenuated by any control action. Since the final steady-state amplitudes are predicted during transient periods, the appropriate control action may be applied at an earlier stage. Experimental data are derived from a rotor/magnetic bearing system and the effectiveness of the transient control is demonstrated.

2. Wavelet analysis

Wavelet analysis provides a multi-scale representation of the time and frequency components within a signal. It has many similarities with Fourier analysis, however, it also offers significant advantages. These include evaluation of frequency components within a time frame without windowing, and practical implementation using filterbanks and digital signal analysis. The wavelet transform of a signal is evaluated by integrating the signal with a mother wavelet $\psi(t)$, where $\psi(t)$ has zero mean and is localised in time. Variation of the translation and dilation of the mother wavelet allows a multi-scale approach. A more detailed explanation can be found in Refs. [19,20]. The continuous wavelet coefficients of system state vector, $\mathbf{x}(t)$, and the input disturbance vector, $\mathbf{f}(t)$, can be expressed as

$$\bar{\mathbf{x}}(\alpha,\tau) = |\alpha|^{-1/2}\int_{-\infty}^{\infty}\mathbf{x}(t)\psi_x\left(\frac{t-\tau}{\alpha}\right)\mathrm{d}t,$$
$$\bar{\mathbf{f}}(\alpha,\tau) = |\alpha|^{-1/2}\int_{-\infty}^{\infty}\mathbf{f}(t)\psi_f\left(\frac{t-\tau}{\alpha}\right)\mathrm{d}t, \quad (1)$$

where the subscripts x and f indicate that the mother wavelets may be different.

In a discrete system the wavelet coefficients are evaluated on a discrete grid. The system state indices α and τ are assigned regularly spaced values $\alpha = mp_0$, and $\tau = nq_0$, where m and n are integer values. It is also possible to evaluate the wavelet coefficients at specific α and τ values using filterbanks. This is achieved by splitting the signal into two parallel channels, filtering one channel with a high-pass filter and the other with a low-pass filter, and downsampling the signals by a factor of 2. The output from the high-pass filter corresponds to the

wavelet coefficients. The output from the low-pass filter can be successively filtered by this process to identify wavelet coefficients at $\alpha = 2^{-a}$ and $\tau = 2^{-a}b$. The discrete time polyphase output signal, $\mathbf{y}'(k)$, from a wavelet filter bank can be expressed as a vector of wavelet coefficients:

$$\mathbf{y}'(k) = [y_1(2^1k), y_2(2^2k), \ldots y_J(2^Jk), y_J(2^Jk+1)]^{\mathrm{T}}. \tag{2}$$

The system and the input disturbance states can be represented in terms of their discrete wavelet coefficients as

$$\mathbf{x}(t) = \mathbf{x}_0 + \sum_{a=0}^{\infty}\sum_{b=0}^{2^a-1} \bar{\mathbf{x}}_d(a,b)\psi_x(2^{-a}t-b),$$
$$\mathbf{f}(t) = \mathbf{f}_0 + \sum_{a=0}^{\infty}\sum_{b=0}^{2^a-1} \bar{\mathbf{f}}_d(a,b)\psi_f(2^{-a}t-b), \tag{3}$$

where $\mathbf{x}_0$ and $\mathbf{f}_0$ are the respective average values of $\mathbf{x}(t)$ and $\mathbf{f}(t)$, and $\bar{\mathbf{x}}_d(a,b) = \bar{\mathbf{x}}(2^{-a}, 2^{-a}b)$ and $\bar{\mathbf{f}}_d(a,b) = \bar{\mathbf{f}}(2^{-a}, 2^{-a}b)$ correspond to the discrete wavelet coefficients. In this paper theoretical simulations and experimental results will consider the Haar wavelet:

$$\psi(t) = \begin{cases} 1, & 0 \leqslant t < 1/2, \\ -1, & 1/2 \leqslant t < 1, \\ 0 & \text{otherwise.} \end{cases} \tag{4}$$

3. Dynamics in the wavelet coefficient domain

By means of an example, consider a single-input single-output dynamic system undergoing a disturbance. The dynamic equation of motion is

$$m\ddot{x}(t) + c\dot{x}(t) + kx(t) = f(t), \tag{5}$$

where m, c and k correspond to the mass, damping and stiffness coefficients, respectively. In order to examine the dynamics in the wavelet transform domain, the continuous wavelet transform of the derivative $\dot{x}(t)$ needs to be identified. Now

$$\bar{\dot{x}}(\alpha,\tau) = |\alpha|^{-1/2}\int_{-\infty}^{\infty} \dot{x}(t)\psi_x\left(\frac{t-\tau}{\alpha}\right)\mathrm{d}t \tag{6}$$

and integration by parts gives

$$\bar{\dot{x}}(\alpha,\tau) = -|\alpha|^{-1/2}\int_{-\infty}^{\infty} x(t)\frac{\partial}{\partial t}\psi_x\left(\frac{t-\tau}{\alpha}\right)\mathrm{d}t. \tag{7}$$

Noting that

$$\frac{\partial}{\partial t}\psi_x\left(\frac{t-\tau}{\alpha}\right) = -\frac{\partial}{\partial \tau}\psi_x\left(\frac{t-\tau}{\alpha}\right)$$

then Eq. (7) can be rearranged as

$$\bar{\dot{x}}(\alpha,\tau) = \frac{\partial}{\partial\tau}\bar{x}(\alpha,\tau) = \bar{x}'(\alpha,\tau), \tag{8}$$

where $(.)'$ denotes partial differentiation with respect to τ. Hence

$$\bar{\ddot{x}}(\alpha,\tau) = \frac{\partial^2}{\partial\tau^2}\bar{x}(\alpha,\tau) = \bar{x}''(\alpha,\tau). \tag{9}$$

The continuous wavelet transform of Eq. (5) now yields

$$m\bar{x}''(\alpha,\tau) + c\bar{x}'(\alpha,\tau) + k\bar{x}(\alpha,\tau) = \bar{f}(\alpha,\tau). \tag{10}$$

Suppose now that $f(t) = H(t)$, the Heaviside step function. The question posed is whether the steady-state response of the system can be extracted by manipulating the wavelet coefficients (Fig. 1). The response of

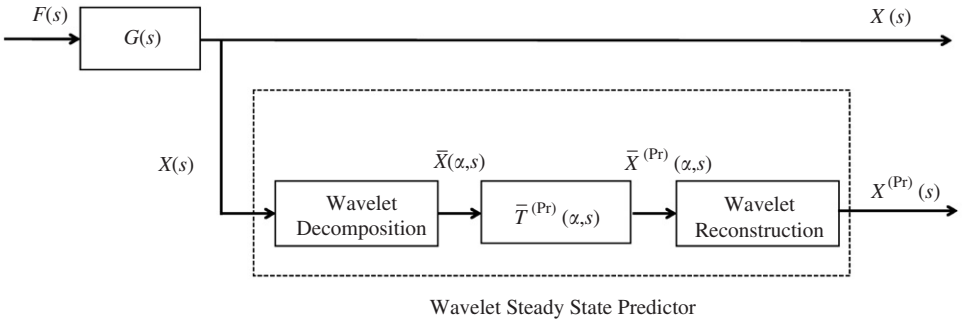

Fig. 1. Block diagram showing predictive steady-state configuration.

the system (5) to an input disturbance can be represented in the Laplace transform domain (with respect to t) as

$$X(s) = G(s)F(s). \tag{11}$$

A similar expression can be used to represent the wavelet coefficient dynamics of Eq. (10) in the Laplace transform domain (with respect to τ) as

$$\bar{X}(\alpha, s) = G(s)\bar{F}(\alpha, s), \tag{12}$$

where the transfer function from input to output for both systems is

$$G(s) = \frac{1}{ms^2 + cs + k}. \tag{13}$$

Expanding the system dynamics using wavelet analysis is seen to identify the system dynamics at different pseudo-frequencies and translations rather than just time, thus allowing transient pseudo-frequencies to be identified.

The objective is to manipulate the wavelet coefficients present in the system response to produce a desired output. This is achieved by removing the original system dynamics and replacing them with a dummy system. In this case the dummy plant is designed to have a faster transient response than the actual system. The wavelet coefficient dynamics of the dummy plant, $\bar{G}^{(\mathrm{Pr})}(\alpha, s)$, to the input disturbance are set as

$$\bar{X}^{(\mathrm{Pr})}(\alpha, s) = \bar{G}^{(\mathrm{Pr})}(\alpha, s)\bar{F}(\alpha, s), \tag{14}$$

where the response $\bar{X}^{(\mathrm{Pr})}(\alpha, s)$ is designed to reach a steady state faster than $\bar{X}(\alpha, s)$. The pertinent transfer function relation is

$$\bar{X}^{(\mathrm{Pr})}(\alpha, s) = \bar{T}^{(\mathrm{Pr})}(\alpha, s)\bar{X}(\alpha, s), \tag{15}$$

where $\bar{T}^{(\mathrm{Pr})}(\alpha, s)$ represents the predictive steady-state transfer function operator. From Eq. (12), $\bar{F}(\alpha, s)$ is given by

$$\bar{F}(\alpha, s) = G^{-1}(s)\bar{X}(\alpha, s). \tag{16}$$

Combining Eq. (16) with Eq. (14) gives

$$\bar{X}^{(\mathrm{Pr})}(\alpha, s) = \bar{G}^{(\mathrm{Pr})}(\alpha, s)G^{-1}(s)\bar{X}(\alpha, s). \tag{17}$$

From Eqs. (15) and (17) the predictive steady-state operator can be identified as

$$\bar{T}^{(\mathrm{Pr})}(\alpha, s) = \bar{G}^{(\mathrm{Pr})}(\alpha, s)G^{-1}(s). \tag{18}$$

The response of the actual and dummy systems to a disturbance may not yield the same steady-state amplitude. However, the steady-state responses can be matched using a scaling term $\Gamma(\alpha)$, which is evaluated

from the final value theorem to yield

$$\lim_{s\to 0} s\bar{X}(\alpha,s) = \Gamma(\alpha)\lim_{s\to 0} s\bar{X}^{(\mathrm{Pr})}(\alpha,s). \tag{19}$$

Hence Eq. (18) is modified to the form

$$\bar{T}^{(\mathrm{Pr})}(\alpha,s) = \Gamma(\alpha)\bar{G}^{(\mathrm{Pr})}(\alpha,s)G^{-1}(s). \tag{20}$$

In practical applications the system plant and prescribed dummy plant may not ensure that $\bar{T}^{(\mathrm{Pr})}(\alpha,s)$ is realisable. To ensure a realisable transfer function $\bar{T}^{(\mathrm{Pr})}(\alpha,s)$ can further be modified to

$$\bar{T}^{(\mathrm{Pr})}(\alpha,s) = \Delta(s)\Gamma(\alpha)\bar{G}^{(\mathrm{Pr})}(\alpha,s)G^{-1}(s). \tag{21}$$

Here

$$\Delta(s) = \frac{1}{(1+\gamma s)^n}, \tag{22}$$

where γ is sufficiently small to ensure that low-frequency response remains the same, but that the high-frequency response of the system is reduced. The integer n must be sufficiently large to ensure that the system is realisable.

To demonstrate this technique consider a simple single-degree-of-freedom system with $m = 0.1$, $c = 0.1$ and $k = 10$ undergoing a step disturbance. The wavelet steady-state predictor is configured to cover a pseudo-frequency range from $1\times$ to $10\times$ the natural frequency of the system, $\omega_n = \sqrt{k/m}$. The Haar wavelet is used to evaluate the wavelet coefficients and is specified in Eq. (4). To evaluate the predictive steady-state transfer function the dummy plant, $\bar{G}^{(\mathrm{Pr})}(\alpha,s)$, must be specified. Define

$$\bar{G}^{(\mathrm{Pr})}(\alpha,s) = \frac{\omega^2_{\mathrm{Pr}}(\alpha)}{s^2 + 2\zeta_{\mathrm{Pr}}(\alpha)\omega_{\mathrm{Pr}}(\alpha)s + \omega^2_{\mathrm{Pr}}(\alpha)}, \tag{23}$$

where $\omega_{\mathrm{Pr}}(\alpha)$ and $\zeta_{\mathrm{Pr}}(\alpha)$ dictate the natural frequency and damping ratio of the dummy system at dilation α. The natural frequencies and damping ratios of the individual plants are specified in Table 1. Evaluating the steady-state amplitudes at each dilation, due to a step input disturbance gives

$$\Gamma(\alpha) = \frac{1}{k}. \tag{24}$$

The full expression for the predictive steady-state wavelet coefficient operator evaluated using Eq. (21) is

$$\bar{T}^{(\mathrm{Pr})}(\alpha,s) = \frac{m\omega^2_{\mathrm{Pr}}(\alpha)s^2 + c\omega^2_{\mathrm{Pr}}(\alpha)s + \omega^2_{\mathrm{Pr}}(\alpha)k}{ks^2 + 2k\omega_{\mathrm{Pr}}(\alpha)\zeta(\alpha)s + k\omega^2_{\mathrm{Pr}}(\alpha)}, \tag{25}$$

where the predictive steady-state transfer function, $\bar{G}^{(\mathrm{Pr})}(\alpha,s)$, is characterised by the natural frequency, $\omega_{\mathrm{Pr}}(\alpha) = 10\omega_n$, and damping ratio, $\zeta_{\mathrm{Pr}}(\alpha) = 1$. This defines a critically damped system capable of responding to higher frequency components present in the disturbance. Fig. 2 shows the system response and the predictive steady state. The corresponding wavelet coefficients are also presented in Fig. 3. The predictive steady state is seen to have a reduced transient settling time. There is a delay associated with the steady-state prediction arising from the evaluation of the wavelet coefficients and the predictive signal reconstruction.

Table 1
Individual system characteristics

Plant	Natural frequency	Damping ratio
System dynamics $G(s)$	ω_n	$\zeta = c/2m\omega_n$
Dummy system wavelet dynamics $\bar{G}^{(\mathrm{Pr})}(\alpha,s)$	$\omega_{\mathrm{Pr}}(\alpha)$	$\zeta_{\mathrm{Pr}}(\alpha)$

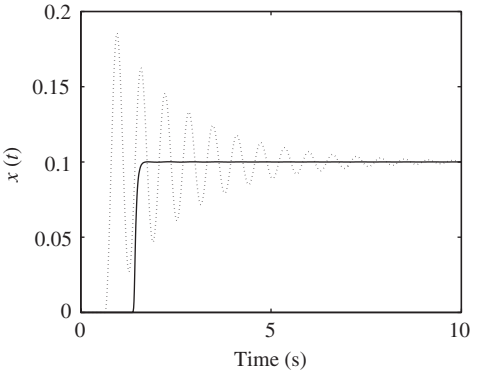

Fig. 2. Direct (dashed line) and predictive steady-state (solid line) simulated system response.

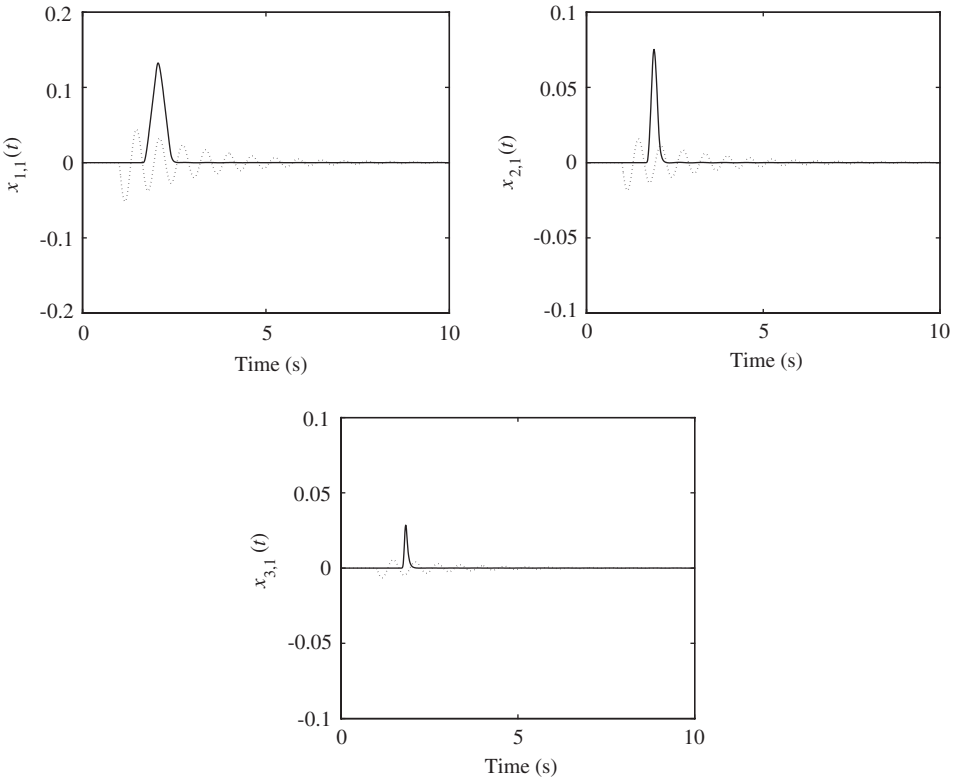

Fig. 3. Direct (dashed line) and predictive steady-state (solid line) wavelet coefficients present in simulated system response.

4. Wavelet steady-state prediction

An example single-input single-output system has been used to demonstrate a method for predicting the steady-state response of a linear system from transient data. The single-input single-output linear system approach can be extended to consider a multi-input multi-output formulation. The system wavelet coefficient and dummy wavelet coefficient plant dynamics (Eqs. (11), (12) and (14)) can be represented as the generalised

multi-input multi-output linear systems

$$\begin{aligned}\mathbf{X}(s) &= \mathbf{G}(s)\mathbf{F}(s),\\ \bar{\mathbf{X}}(\alpha,s) &= \bar{\mathbf{G}}(\alpha,s)\bar{\mathbf{F}}(\alpha,s),\\ \bar{\mathbf{X}}^{(\mathrm{Pr})}(\alpha,s) &= \bar{\mathbf{G}}^{(\mathrm{Pr})}(\alpha,s)\bar{\mathbf{F}}(\alpha,s),\end{aligned} \tag{26}$$

where the wavelet system transfer function, $\bar{\mathbf{G}}(\alpha,s)$, is now dependent on the pseudo-frequency, α. This allows nonlinear variations with α to be included.

The predictive steady-state operator specified in Eq. (20) becomes the multi-input multi-output transfer function

$$\bar{\mathbf{T}}^{(\mathrm{Pr})}(\alpha,s) = \Gamma(\alpha)\bar{\mathbf{G}}^{(\mathrm{Pr})}(\alpha,s)\bar{\mathbf{G}}^{*}(\alpha,s), \tag{27}$$

where $\bar{\mathbf{G}}^{*}(\alpha,s)$ is the pseudo-inverse of $\bar{\mathbf{G}}(\alpha,s)$ satisfying $\bar{\mathbf{G}}^{*}(\alpha,s)\bar{\mathbf{G}}(\alpha,s) = \mathbf{I}$ and $\Gamma(\alpha)$ is identified from

$$\lim_{s\to 0} s\bar{\mathbf{X}}(\alpha,s) = \Gamma(\alpha)\lim_{s\to 0} s\bar{\mathbf{X}}^{(\mathrm{Pr})}(\alpha,s). \tag{28}$$

For practical use $\bar{\mathbf{T}}^{(\mathrm{Pr})}(\alpha,s)$ is required to be fully realisable. This can be ensured by modifying the transfer function as

$$\bar{\mathbf{T}}^{(\mathrm{Pr})}(\alpha,s) = \mathbf{\Delta}(s)\Gamma(\alpha)\bar{\mathbf{G}}^{(\mathrm{Pr})}(\alpha,s)\bar{\mathbf{G}}^{*}(\alpha,s), \tag{29}$$

where

$$\mathbf{\Delta}(s) = \frac{1}{(1+\gamma s)^{n}}\mathbf{I}, \tag{30}$$

where γ and n have already been described. This forms the basis for a method predicting the steady-state vibration response of a multi-input multi-output system.

5. Discrete rotor dynamics

A continuous time approach may be undertaken to identify the relationships between the following variables:

$$\begin{aligned}&\mathbf{f}(t) \to \mathbf{F}(s),\\ &\mathbf{x}(t) \to \mathbf{X}(s),\\ &\bar{\mathbf{f}}(\alpha,\tau) \to \bar{\mathbf{F}}(\alpha,s),\\ &\bar{\mathbf{x}}(\alpha,\tau) \to \bar{\mathbf{X}}(\alpha,s),\end{aligned} \tag{31}$$

where the response of a generalised linear system can be evaluated from superposing $2N$ individual modal contributions:

$$\mathbf{X}(s) = \sum_{l=1}^{2N} \frac{1}{s-\lambda_l}\mathbf{G}_l\mathbf{F}(s). \tag{32}$$

For practical applications a filterbank approach will be used. The system response and disturbance can be represented in discrete time ($t \to kT$ and $\tau \to 2^{-a}b$). The discrete sequences $\{\mathbf{f}_d(kT) : k = 0,1,2,\ldots\}$, $\{\mathbf{x}_d(kT) : k = 0,1,2,\ldots\}$, $\{\bar{\mathbf{f}}_d(a,b) : b = 0,1,2,\ldots\}$ and $\{\bar{\mathbf{x}}_d(p,q) : b = 0,1,2,\ldots\}$ may be represented by the Z-transforms $\mathbf{F}_d(z)$, $\mathbf{X}_d(z)$, $\bar{\mathbf{F}}_d(z,a)$ and $\bar{\mathbf{X}}_d(z,p)$, respectively. Here the subscript d signifies variables defined in discrete time. The associated transfer functions are shown in the Appendix.

6. Wavelet coefficient predictive steady-state control moderation

Wavelet decomposition allows for the identification of wavelet coefficients corresponding to specific frequency bandwidths present in the measured rotor vibration. Conversely, wavelet reconstruction can be used to create control signals from wavelet coefficients acting to suppress amplitudes over a specified vibration bandwidth. Applying a control strategy in the wavelet coefficient domain allows for loop shaping of the wavelet coefficients. This provides a method of control targeting specific components within the measured signal. A proportional controller is proposed to provide control action in the wavelet coefficient domain, acting on a specific wavelet coefficient. To overcome control instabilities during transient excitation, and to assess improvements in controller performance, steady-state prediction will be used to moderate the control signal. The control force can be evaluated in the wavelet coefficient Z-transform domain as $\bar{\mathbf{U}}(p,z) = -\bar{\mathbf{L}}(p,z)\bar{\mathbf{X}}_d(p,z)$ where $\bar{\mathbf{L}}(p,z) = k(p)$ defines a proportional control action. The closed loop response of the system incorporating negative feedback can now be identified as

$$(\mathbf{I} - \bar{\mathbf{G}}(a,p,z)\mathbf{B}_u\bar{\mathbf{L}}(p,z))\bar{\mathbf{X}}_d(p,z) = \bar{\mathbf{G}}_0(a,z)\mathbf{f}_0 - \sum_{a=0}^{\infty}\bar{\mathbf{G}}(a,p,z)\bar{\mathbf{F}}_d(a,z), \tag{33}$$

where $\mathbf{B}_u$ is a distribution matrix matching the output states to the control force. $\bar{\mathbf{G}}_0(a,z)$ is the transfer function relating a constant input disturbance over a fixed time period to the measured rotor displacement. $\bar{\mathbf{G}}(a,p,z)$ relates wavelet coefficients present in the input disturbance to the wavelet coefficients in the rotor vibration. In the case of the proportional predictive steady-state controller the wavelet control coefficients will take the form $\bar{\mathbf{U}}(p,z) = -\bar{\mathbf{L}}(p,z)\bar{\mathbf{T}}^{(\mathrm{Pr})}(p,z)\bar{\mathbf{X}}_d(p,z)$, where $\bar{\mathbf{T}}^{(\mathrm{Pr})}(p,z)$ is the discrete time predictive steady-state transfer function. Therefore, with steady-state prediction equation (33) becomes

$$(\mathbf{I} - \bar{\mathbf{G}}(a,p,z)\mathbf{B}_u\bar{\mathbf{L}}(p,z)\bar{\mathbf{T}}^{(\mathrm{Pr})}(p,z))\bar{\mathbf{X}}_d(p,z) = \bar{\mathbf{G}}_0(a,z)\mathbf{f}_0 - \sum_{a=0}^{\infty}\bar{\mathbf{G}}(a,p,z)\bar{\mathbf{F}}_d(a,z). \tag{34}$$

In practice, implementation of a wavelet coefficient domain controller will result in evaluation delays between the disturbance measurement and control force. Incorporating delays modifies the controller transfer function to $\bar{\mathbf{L}}(p,z) = k(p)\mathbf{I}z^{-i}$, where i is the number of cycles over which the control signal is evaluated. This can also be used to incorporate any delays associated with the evaluation of the predicted steady-state vibration. The closed loop system response with controller evaluation delays can be expressed as

$$(\mathbf{I} - \bar{\mathbf{G}}(a,p,z)\mathbf{B}_u k(p)z^{-i}\bar{\mathbf{T}}^{(\mathrm{Pr})}(p,z))\bar{\mathbf{X}}_d(p,z) = \bar{\mathbf{G}}_0(a,z)\mathbf{f}_0 - \sum_{a=0}^{\infty}\bar{\mathbf{G}}(a,p,z)\bar{\mathbf{F}}_d(a,z). \tag{35}$$

7. Experimental validation

7.1. Experimental facility

An experimental flexible rotor/active magnetic bearing facility (Fig. 4) was used to validate the predictive steady-state detection strategy. The rotor was 2 m long, 50 mm in diameter, and 60 kg in mass. Four 10 kg disks were located along the rotor to reduce the natural frequencies of the first two bending modes to below the maximum operating speed of the motor, 6000 rev/min. Radial forces were applied through two active magnetic bearings, each constructed from eight poles forming two orthogonal opposing coil pairs. These were positioned at $\pm 45^\circ$ to the vertical to maximise static load. The maximum radial force exerted by a single magnetic bearing was 1700 N before roll-off at 100 Hz. Rotor displacement relative to base motion was measured using eight eddy-current sensors, formed into four orthogonal pairs. The four sensor planes were positioned at the rotor ends and adjacent to the active magnetic bearings. Sensor feedback from the central measurement planes was used in conjunction with a local proportional–integral–derivative (PID) control

strategy to allow stable levitation of the rotor. The rotor modes of vibration are 10 Hz (near rigid body conical whirl), 19 Hz (near rigid cylindrical body whirl), 28 Hz (dominant first-order bending) and 67 Hz (dominant second-order bending). The corresponding damping ratios are 0.20, 0.13, 0.085, and 0.085, respectively.

The modal matrix $\mathbf{G}_l$ specified in Eq. (32) relates a disturbance force vector $\mathbf{F}$ of dimension n_f to a rotor displacement vector $\mathbf{X}$ of dimension n_x. In principle, $\mathbf{G}_l$ could be derived from dynamic equations, for example, based on finite element methods. However, the control action specified in the left-hand side

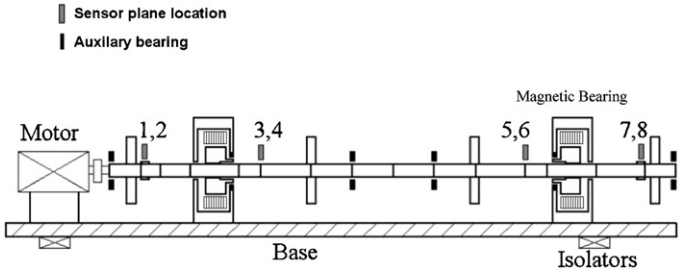

Fig. 4. Schematic diagram of an experimental flexible rotor supported by two active magnetic bearings.

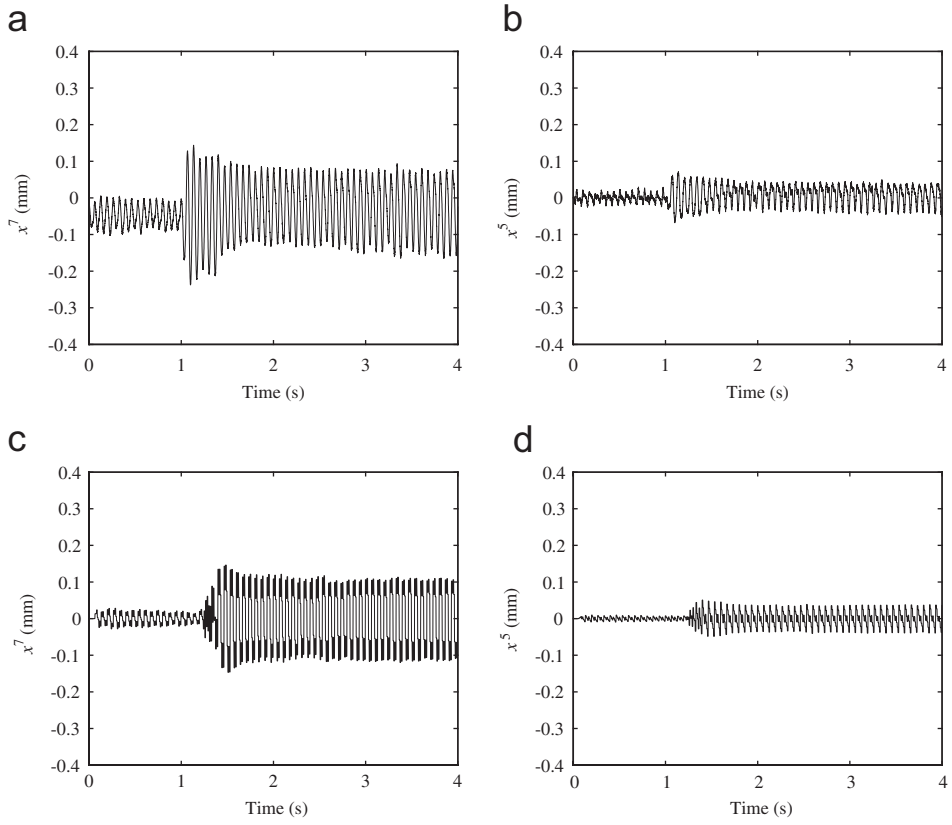

Fig. 5. Measured and predictive steady-state mass-loss responses in the x-axis at the non-driven end disk (x^7) and non-driven end active magnetic bearing (x^5) at a rotational speed of 15 Hz. (a,b) show the measured response, (c,d) show the predictive steady-state response.

of Eq. (33) involves the matrix $\mathbf{G}_l\mathbf{B}_u$. The matrix $\mathbf{B}_u$ extracts the columns of $\mathbf{G}_l$ that are relevant only to the control force vector (of dimension 4 for the experimental system). The relevant columns of $\mathbf{G}_l$ may therefore be obtained through online signal processing and identification based on known inputs applied through magnetic bearings and measured rotor displacement signals. This was the approach adopted in this paper.

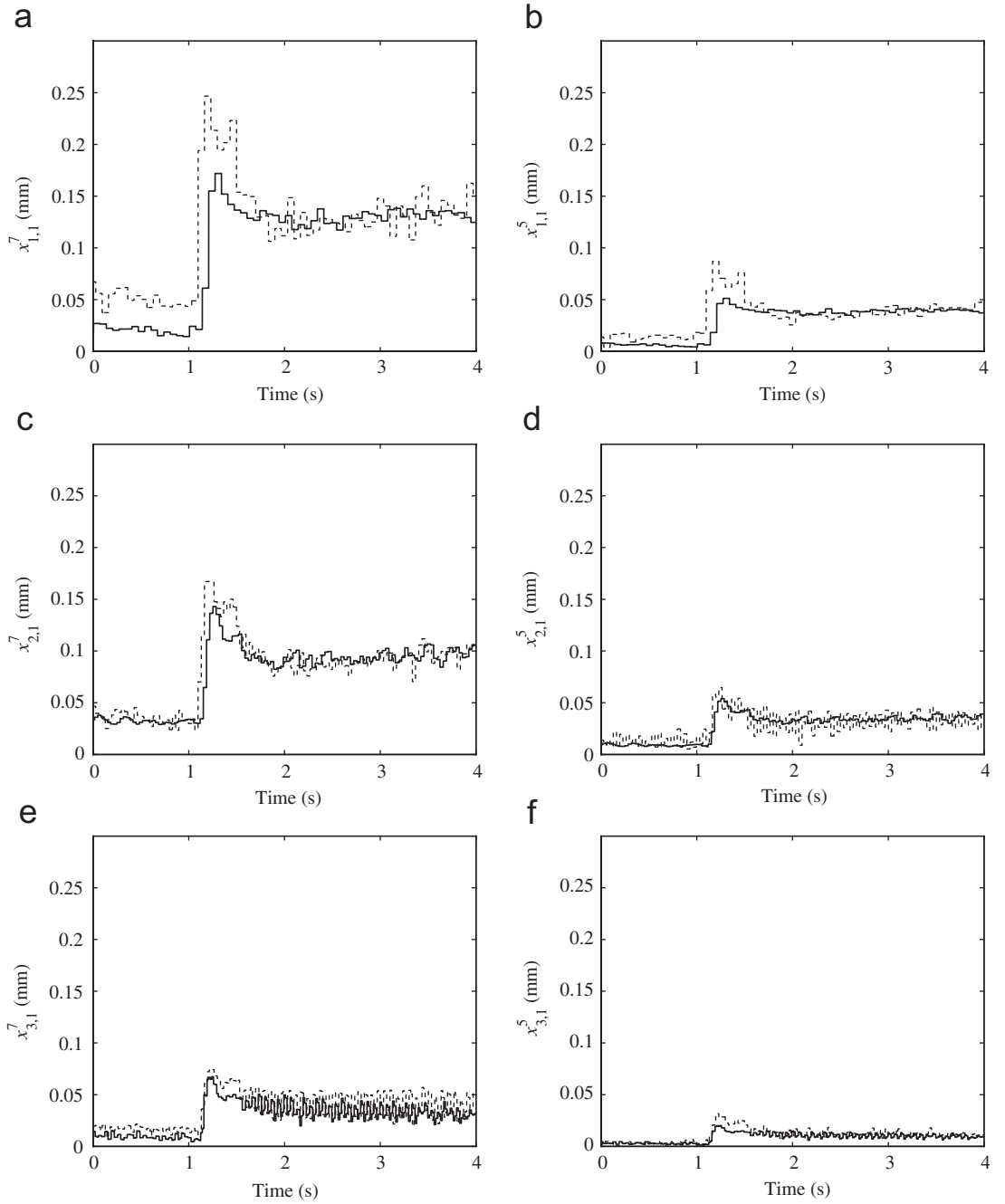

Fig. 6. Measured direct (dashed line) and predictive steady-state (solid line) wavelet coefficient responses in the x-axis at the non-driven end (x^7) disk and non-driven end active magnetic bearing (x^5) corresponding to 1× (a,b), 2× (c,d) and 4× (e,f) the rotational speed.

7.2. Experimental procedure and results

Experimental validation of the wavelet coefficient predictive steady state and control strategy was performed using mass-loss tests at a rotational speed of 15 Hz. These were used to induce step changes in rotor unbalance from an initially indeterminate state. Mass-loss was induced by cutting free an attached mass at the non-driven end disk using a blade mechanism. The effective mass loss eccentricity was 196 gcm. The steady-state predictor was configured with three wavelet coefficient levels and pseudo-frequencies corresponding to 1×, 2× and 4× the rotational speed of the rotor. The Haar wavelet was used to evaluate the wavelet coefficients and is specified in Eq. (4). The filterbank sampling time was specified as $T = 1/(2^i\Omega)$, where i indicates the wavelet pseudo-frequency level relative to the synchronous frequency, Ω. The inverse transfer function used with predictive steady state was identified from on-line measurement and truncated after 5 time steps to allow for efficient real-time implementation. The decomposition filterbank residue was set to zero. This removes any constant component from the signal. Therefore, predictive steady-state signal processing identifies the steady-state vibrational amplitude of the system to a step change in the synchronous harmonic disturbance only. The response of the rotor due to mass-loss at 15 Hz is shown in Fig. 5 along with the predictive steady-state response. The measured direct and predictive wavelet coefficient values corresponding to 1×, 2× and 4× the rotational frequency are presented in Fig. 6.

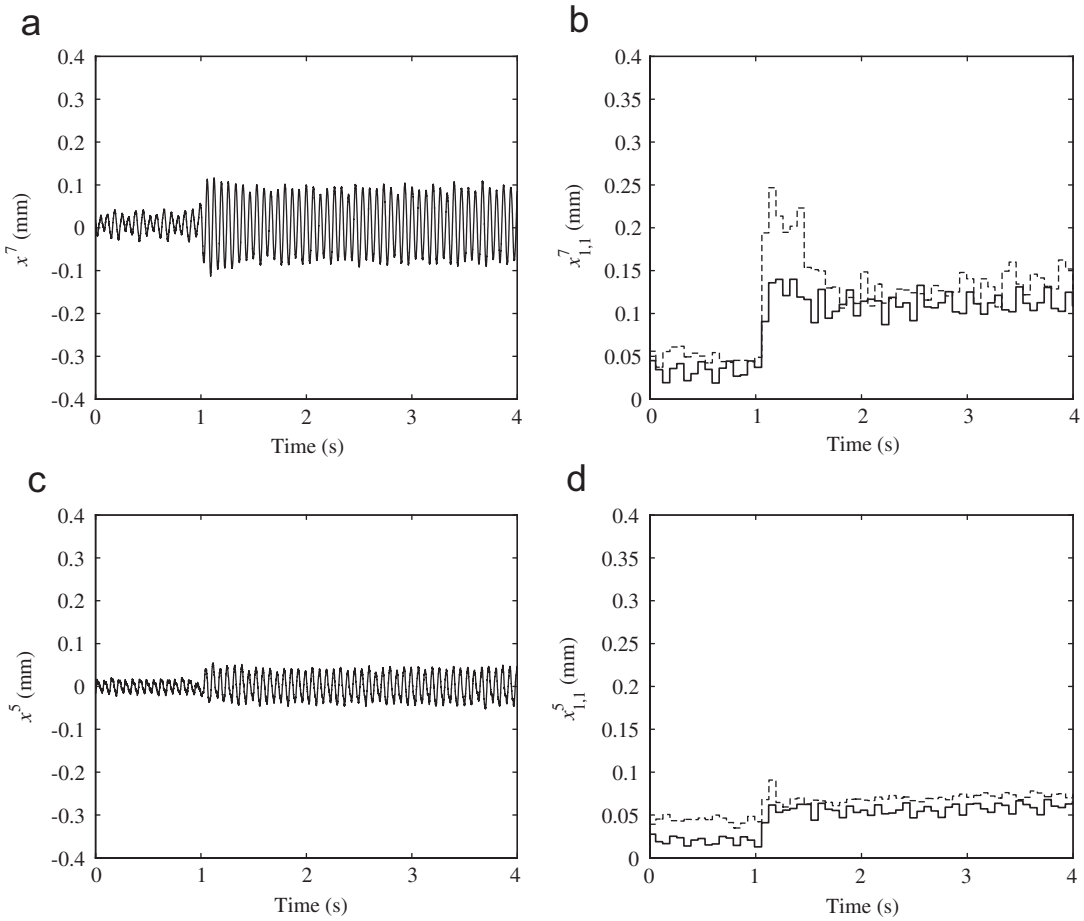

Fig. 7. Measured mass-loss response (a,c) in the x-axis at a rotational speed of 15 Hz using proportional wavelet controller C1. Wavelet coefficients corresponding to 1× the rotational frequency with controller C1 (solid) and basic PID controlled (dashed) cases (b,d).

Two wavelet coefficient controllers were implemented:

(C1) With proportional wavelet coefficient feedback.
(C2) With proportional wavelet coefficient feedback moderated using predictive steady-state wavelet coefficients.

To minimise the number of variables and allow direct comparison, both controllers were configured using a single wavelet coefficient level. The wavelet controller evaluation time corresponded to a 3 cycle delay. Controller stability was assessed using an acceptability bound on performance. A controller was defined as unacceptable if the rotor displacement exceeded a specified limit, 0.5 mm, in any control plane. The acceptable upper limits of the proportional gains were $k_{1,1} = 0.41$ and $k_{1,1} = 0.68$ for controllers (C1) and (C2), respectively. To assess controller performance a wavelet coefficient feedback gain corresponding to 50% of the maximum acceptable limit was used. The rotor displacement and corresponding wavelet coefficients in the x-axis for the uncontrolled case have already been presented in Figs. 5 and 6. Figs. 7 and 9 show the rotor displacement in the x-axis for using the proportional wavelet coefficient controller (C1) and the proportional wavelet controller with predictive steady-state moderation (C2). The corresponding control forces are presented in Figs. 8 and 10. Mass-loss experiments show that both controllers suppress rotor vibration. In the

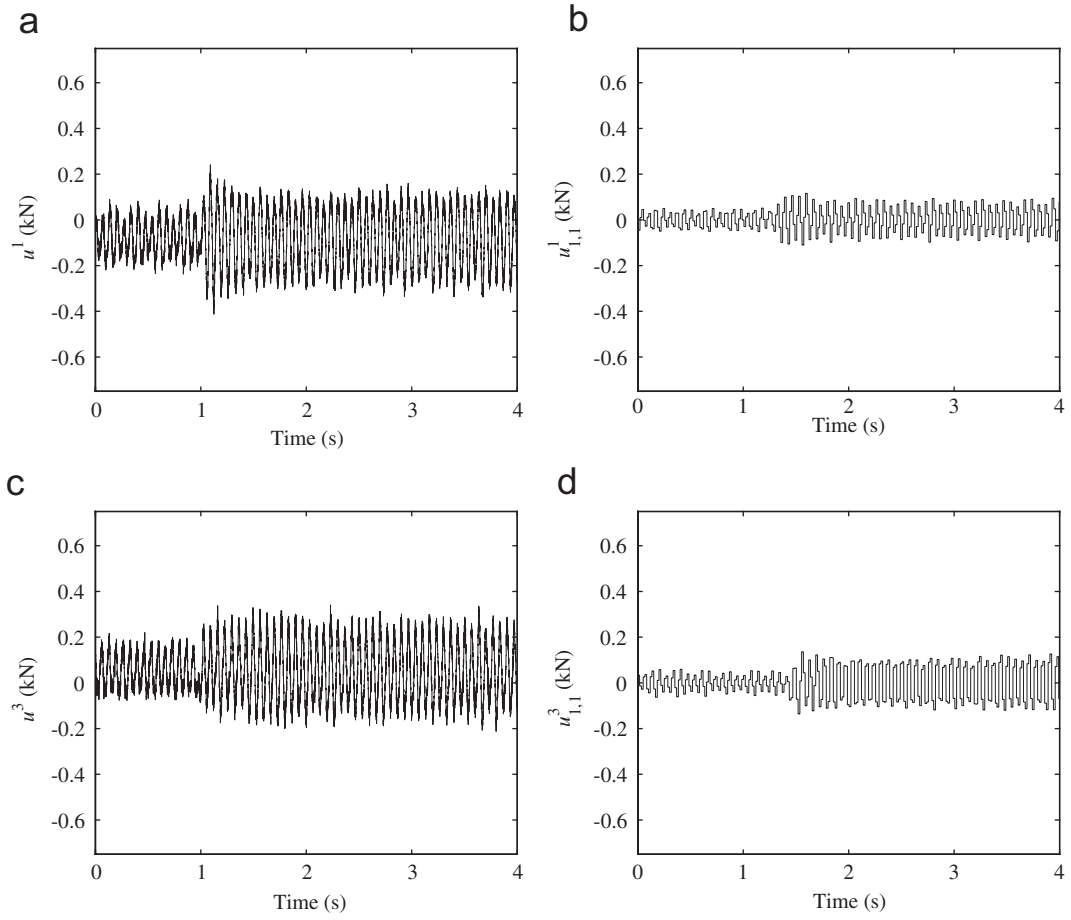

Fig. 8. (a) and (c) show the total control forces at non-driven end and non-driven end active magnetic bearings at a rotational speed of 15 Hz; (b) and (d) show the wavelet coefficients used to form the control force.

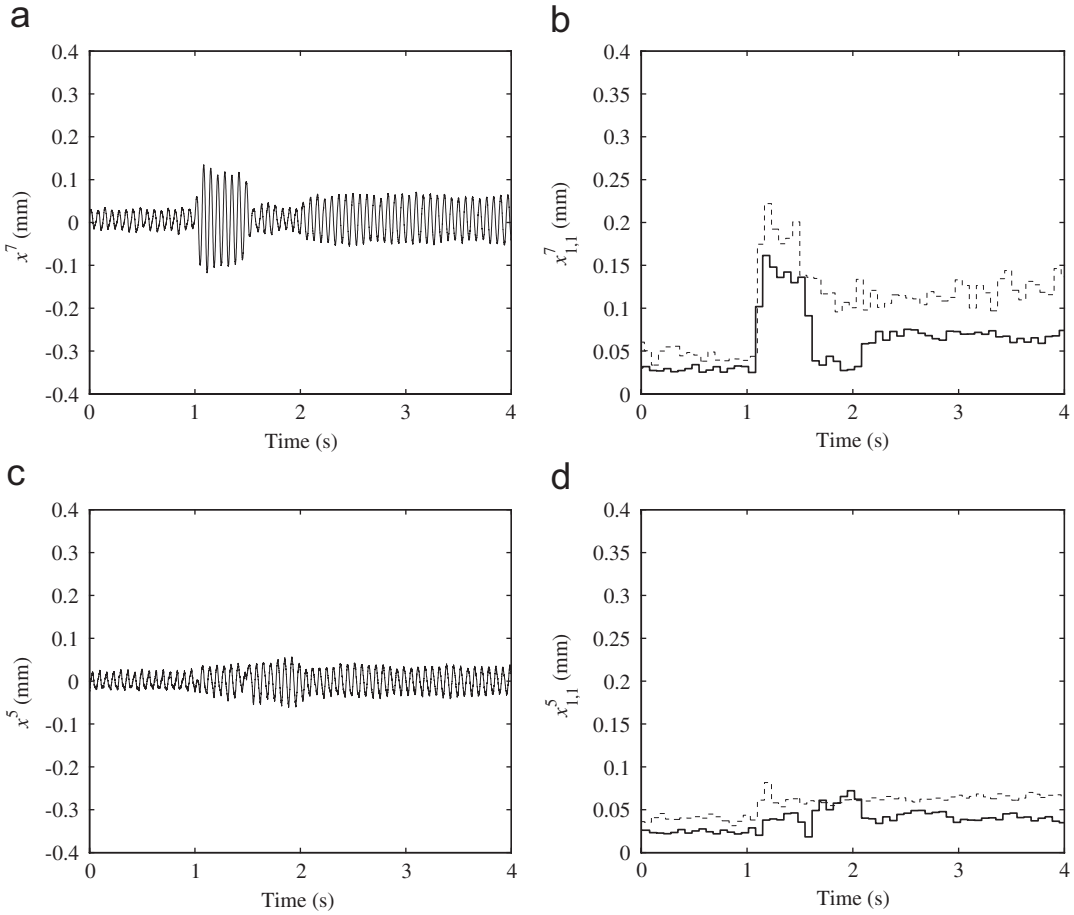

Fig. 9. Measured mass-loss response (a,c) in the x-axis at a rotational speed of 15 Hz using wavelet controller C2. Wavelet coefficients corresponding to 1× the rotational frequency with controller C2 (solid) and basic PID controlled (dashed) cases (b,d).

case of direct wavelet coefficient feedback the lower stability boundary results in a conservative control strategy. Moderating the controller input using predictive steady-state measurements increases the stability boundary allowing for improved system performance. Predictive steady-state moderation is therefore seen as an improvement to the control of the system allowing for better control action when transient vibration occurs [Figs. 7–10].

8. Conclusions

A method of identifying the steady-state vibration of a generalised linear system using wavelet coefficients has been presented. Experimental validation of the technique was performed using a flexible rotor/active magnetic bearing assembly. Mass-loss tests were used to provide sudden changes in the synchronous disturbance resulting in responses containing transient vibration. Results indicate that this method provides an accurate estimation of the steady-state response during the transient phase. In a discrete time approach the disturbance can be represented as a summation of appropriate step changes. Therefore it follows that the predictive steady-state method can be applied to consider any system disturbance.

A simple proportional wavelet coefficient controller was introduced as a means of targeting specific rotor vibration. A second controller was identified using predictive steady-state techniques to moderate the wavelet coefficient. Experimental validation of the controllers was performed using mass-loss tests. Both controllers

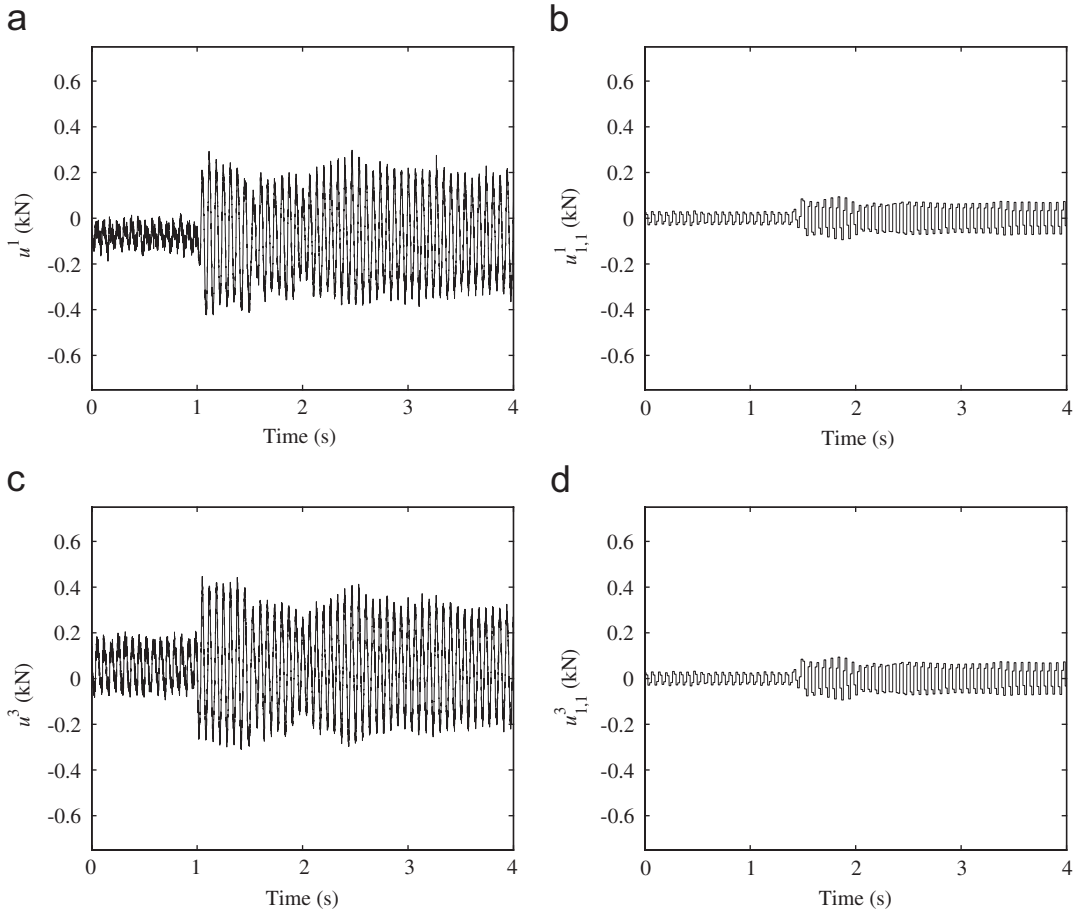

Fig. 10. (a) and (c) show the total control forces at non-driven end and non-driven end active magnetic bearings at a rotational speed of 15 Hz; (b) and (d) show the wavelet coefficients used to form the control force.

reduced rotor vibration. However, the controller incorporating predictive steady-state vibration improved closed loop stability allowing for improved performance during transient vibration.

Acknowledgements

The authors gratefully acknowledge the funding support of the Engineering and Physical Sciences Research Council through Grant GR/R45277/01.

Appendix A. Wavelet coefficients relation between rotor vibration and input disturbance

The Laplace transform of the input disturbance, $\mathbf{f}(t)$, can be expressed in terms of the wavelet coefficient series as

$$\mathbf{F}(s) = \int_0^\infty \left[\mathbf{f}_0 + \sum_{a=0}^{\infty} \sum_{b=0}^{2^a-1} \mathbf{f}_d(a,b)\psi(2^{-a}t - b) \right] \mathrm{e}^{-st}\,\mathrm{d}t. \tag{A.1}$$

Define

$$e_1(s) = \frac{1}{s} \tag{A.2}$$

and

$$e_2(s,a,b) = \int_0^\infty \psi(2^{-a}t - b)\mathrm{e}^{-st}\,\mathrm{d}t, \tag{A.3}$$

$e_1(s)$ relates to the Laplace transform of the average input disturbance, $\mathbf{f}^0$. $e_2(s,a,b)$ represents the Laplace transform of the mother wavelet at a specific translation and dilation. The Laplace transform of the input disturbance can then be simplified to

$$\mathbf{F}(s) = \mathbf{f}_0 e_1(s) + \sum_{a=0}^{\infty}\sum_{b=0}^{2^a-1} \bar{\mathbf{f}}_d(a,b) e_2(s,a,b). \tag{A.4}$$

The response of the system can be evaluated by superposing the individual modal contributions. From Eq. (32), the Laplace transform of the system states can be evaluated in terms of the input disturbance wavelet coefficients as

$$\mathbf{X}(s) = \sum_{l=1}^{2N} \frac{\mathbf{G}_l}{s-\lambda_l}\left[\mathbf{f}_0 e_1(s) + \sum_{a=0}^{\infty}\sum_{b=0}^{2^a-1} \bar{\mathbf{f}}_d(a,b) e_2(s,a,b)\right]. \tag{A.5}$$

Poles exist at $s = 0$ and $s = \lambda_l$. Therefore, the inverse Laplace transform gives the dynamic system response in the form

$$\mathbf{x}(t) = \sum_{l=1}^{2N} \mathbf{G}_l\left[\mathbf{f}_0 u_1(t,\lambda_l) + \sum_{a=0}^{\infty}\sum_{b=0}^{2^a-1} \bar{\mathbf{f}}_d(a,b) u_2(t,\lambda_l,a,b)\right], \tag{A.6}$$

where

$$\begin{aligned} u_1(t,\lambda_l) &= \mathscr{L}^{-1}\left[\frac{e_1(s)}{(s-\lambda_l)}\right] = \mathscr{L}^{-1}\left[\frac{1}{s(s-\lambda_l)}\right] = \frac{1}{\lambda_l}(1-\mathrm{e}^{\lambda_l t}),\\ u_2(t,\lambda_l,a,b) &= \mathscr{L}^{-1}\left[\frac{1}{s-\lambda_l} e_2(s,a,b)\right]. \end{aligned} \tag{A.7}$$

Here $\mathscr{L}^{-1}[.]$ indicates the inverse Laplace transform. The relation between the wavelet coefficients of the input disturbance and the system states can be realised from the wavelet transform of $\mathbf{x}(t)$. Define

$$\begin{aligned} g_1(\lambda_l,p,q) &= |2^{-p}|^{-1/2}\int_{-\infty}^{\infty} u_1(t,\lambda_l)\psi(2^{-p}t-q)\,\mathrm{d}t,\\ g_2(\lambda_l,a,b,p,q) &= |2^{-p}|^{-1/2}\int_{-\infty}^{\infty} u_2(t,\lambda_l,a,b)\psi(2^{-p}t-q)\,\mathrm{d}t. \end{aligned} \tag{A.8}$$

Eq. (A.6) can be transformed into the wavelet coefficient domain as:

$$\bar{\mathbf{x}}_d(p,q) = \sum_{l=1}^{2N} \mathbf{G}_l\left[\mathbf{f}_0 g_1(\lambda_l,p,q) + \sum_{a=0}^{\infty}\sum_{b=0}^{2^a-1} \bar{\mathbf{f}}_d(a,b) g_2(\lambda_l,a,b,p,q)\right]. \tag{A.9}$$

The summation term, over disturbance time index b, in Eq. (A.9) represents the convolution of the system dynamics with the disturbance wavelet coefficient. The discrete sequences $\{\bar{\mathbf{x}}_d(p,q) : q = 0,1,2,\ldots\}$, $\{\bar{\mathbf{f}}_d(a,b) : b = 0,1,2,\ldots\}$, $\{g_1(\lambda_l,p,q) : q = 0,1,2,\ldots\}$, and $\{g_2(\lambda_l,a,b,p,q) : q = 0,1,2,\ldots\}$ may be represented by Z-transforms $\bar{\mathbf{X}}_d(p,z)$, $\bar{\mathbf{F}}_d(a,z)$, $G_1(\lambda_l,p,z)$ and $G_2(\lambda_l,a,p,z)$, respectively. The relation between the input disturbance wavelet coefficients and the system states wavelet coefficients can now be expressed as

$$\bar{\mathbf{X}}_d(p,z) = \bar{\mathbf{G}}_0(p,z)\mathbf{f}_0 - \sum_{a=0}^{\infty} \bar{\mathbf{G}}(a,p,z)\bar{\mathbf{F}}_d(a,z), \tag{A.10}$$

where

$$\bar{\mathbf{G}}_0(p,z) = \sum_{l=1}^{2N} \mathbf{G}_l G_1(\lambda_l, p, z),$$

$$\bar{\mathbf{G}}(a,p,z) = \sum_{l=1}^{2N} \mathbf{G}_l G_2(\lambda_l, a, p, z). \tag{A.11}$$

References

[1] C.R. Burrows, M.N. Sahinkaya, Vibration control of mutli-mode rotor-bearing systems, *Proceedings of the Royal Society of London Series A—Mathematical Physical and Engineering Sciences* 386 (1790) (1983) 74–94.

[2] B. Sahfai, B. Beale, P. LaRocca, E. Cussons, Magnetic bearing control systems and adaptive forced balancing, *Control Systems IEEE* 14 (1994) 4–113.

[3] C.R. Knospe, R.W. Hope, S.J. Fedigan, R.D. Williams, Experiments in the control of unbalance response using magnetic bearings, *Mechatronics* 5 (4) (1995) 385–400.

[4] M. Fujita, F. Matsumura, M. Shimizu, Robust control design for a magnetic suspension system, *Proceedings of the Second International Symposium on Magnetic Bearings*, 1990, pp. 349–356.

[5] M.O.T. Cole, P.S. Keogh, C.R. Burrows, Vibration control of a flexible rotor magnetic bearing system subject to direct forcing and base motion disturbances, *Proceedings of the Institution of Mechanical Engineers Part C: Journal of Mechanical Engineering Science* 212 (7) (1998) 535–546.

[6] P.S. Keogh, C. Mu, C.R. Burrows, Optimized design of vibration controllers for steady and transient excitation of flexible rotors, *Proceedings Institute of Mechanical Engineers Part C: Journal of Mechanical Engineering Science* 209 (3) (1995) 155–168.

[7] K. Nonami, T. Ito, μ synthesis of flexible rotor magnetic bearing systems, *Proceedings of the Fourth International Symposium on Magnetic Bearings*, 1994, pp. 73–78.

[8] D.E. Newland, Wavelet analysis of vibration, part 1: theory, *Journal of Vibration and Acoustics—Transactions of the ASME* 116 (4) (1994) 409–416.

[9] D.E. Newland, Wavelet analysis of vibration, part 2: wavelet maps, *Journal of Vibration and Acoustics—Transactions of the ASME* 116 (4) (1994) 417–425.

[10] W.J. Staszewski, Identification of damping in MDOF systems using time-scale decomposition, *Journal of Sound and Vibration* 203 (2) (1997) 283–305.

[11] W.J. Staszewski, Identification of non-linear systems using multi-scale ridges and skeletons of the wavelet transform, *Journal of Sound and Vibration* 214 (4) (1998) 639–658.

[12] V.C. Chancey, G.T. Flowers, Identification of transient vibration characteristics using absolute harmonic wavelet coefficients, *Journal of Vibration and Control* 7 (8) (2001) 1175–1193.

[13] J. Zou, K. Chen, J.C. Niu, Z.M. Geng, Study on the transient response and wavelet time–frequency feature of a cracked rotor passing through a subcritical speed, *Journal of Strain Analysis for Engineering Design* 38 (3) (2003) 269–276.

[14] I.S. Cade, P.S. Keogh, M.N. Sahinkaya, Fault identification in rotor/magnetic bearing systems using discrete time wavelet coefficients, *IEEE– ASME Transactions on Mechatronics* 10 (6) (2005) 648–657.

[15] Z. Geng, L. Qu, Vibrational diagnosis of machine parts using the wavelet packet technique, *British Journal of Non-Destructive Testing* 36 (1) (1994) 11–15.

[16] J. Lin, L.S. Qu, Feature extraction based on Morlet wavelet and its application for mechanical fault diagnosis, *Journal of Sound and Vibration* 234 (1) (2000) 135–148.

[17] S. Parvez, Z.Q. Goa, A wavelet-based multiresolution PID controller, *IEEE Transactions on Industry Applications* 41 (2) (2005) 537–543.

[18] M.O.T. Cole, P.S. Keogh, C.R. Burrows, M.N. Sahinkaya, Wavelet domain control of rotor vibration, *Proceedings of the Institution of Mechanical Engineers, Part C: Journal of Mechanical Engineering Science* 220 (2) (2006) 167–184.

[19] G. Strang, T. Nguyen, *Wavelets and Filter Banks*, Wellsey-Cambridge Press, Cambridge, MA, 1996.

[20] M. Vetterli, J. Kovačević, *Wavelets and Subband Coding*, Prentice-Hall, Inc., Englewood Cliffs, NJ, 1995.